Systems pharmacology of the amyloid cascade : unfolding oligomer modulation in Alzheimer's disease

Maanen, E.M.T. van

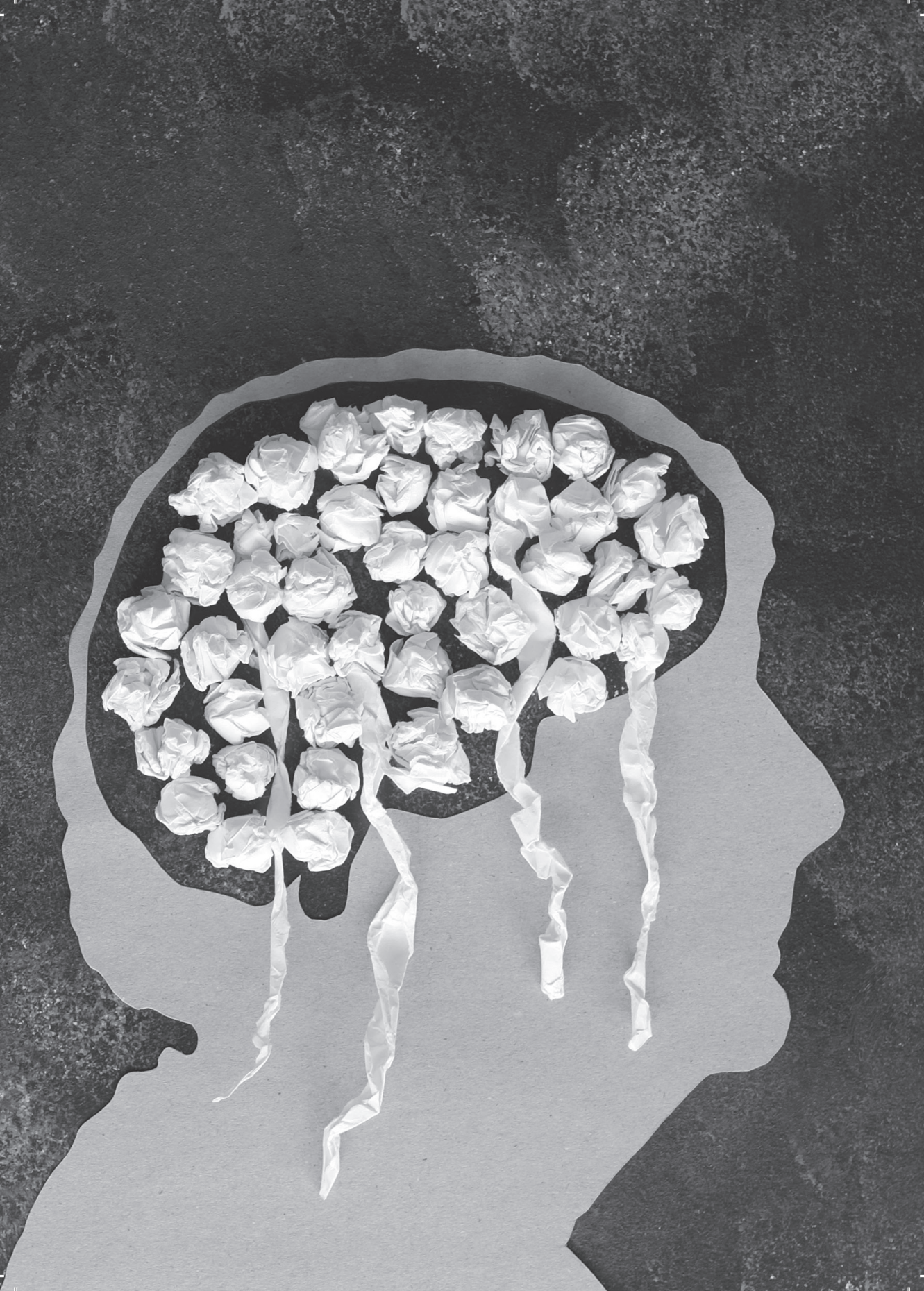

Chapter 5

Extending a systems model of the APP pathway: Separation of β- and γ-secretase sequential cleavage steps of APP

E.M.T. van Maanen, T.J. van Steeg, M.J. Ahsman, M.S. Michener, M.J. Savage, M.E. Kennedy, H.J. Kleijn, J.A. Stone, M. Danhof

Submitted to JPET

Visual Abstract

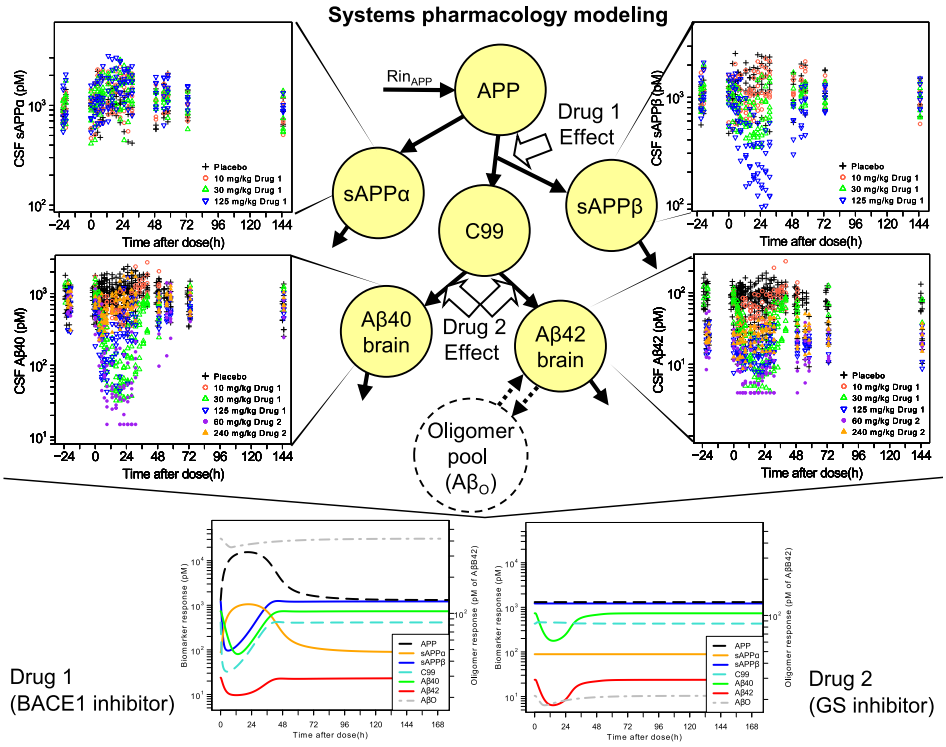

Abstract

The abnormal accumulation of amyloid-β (Aβ) in the brain parenchyma has been posited as a central event in the pathophysiology of Alzheimer's disease. Recently, we have proposed a systems pharmacology model of the APP pathway, describing the Aβ precursor protein (APP) metabolite responses (Aβ40, Aβ42, sAPPα and sAPPβ) to β-secretase 1 (BACE1) inhibition[1]. In this investigation this model was challenged to describe Aβ dynamics following γ-secretase (GS) inhibition. This led an extended systems pharmacology model, with separate descriptions to characterize the sequential cleavage steps of APP by BACE1 and GS, to describe the differences in Aβ response to their respective inhibition. Following GS inhibition a lower Aβ40 formation rate constant was observed, compared to BACE1 inhibition. Both BACE1 and GS inhibition were predicted to lower Aβ_{O} levels. Further model refinement and new data may be helpful to fully understand the difference in Aβ dynamics following BACE1 *versus* GS inhibition.

Introduction

The amyloid cascade hypothesis posits that the pathological cascade leading to Alzheimer's Disease (AD) is triggered by abnormal accumulation of amyloid-β protein (Aβ) in the brain parenchyma[2]. Inhibition of Aβ production in the brain is therefore a therapeutic target for treating AD with a potentially disease-modifying effect[3,4].

Aβ is generated through sequential proteolytic cleavage of β-amyloid precursor protein (APP) by β-secretase (BACE1) and γ-secretase (GS)[5], as schematically depicted in Figure 5.1. In the first cleavage step, the N-terminal secreted fragment soluble APPβ (sAPPβ) and the C-terminal membrane-bound 99-amino acid fragment (βCTF or C99) are formed by BACE1. Subsequently, C99 is cleaved by GS yielding Aβ species of different chain length of which Aβ38, Aβ40 and Aβ42 are the most common isoforms. In an alternative pathway, cleavage of APP by α-secretase leads to the formation of soluble APPα (sAPPα) and the C-terminal membrane-bound 83-amino acid fragment (αCTF or C83). α-secretase cleavage precludes Aβ formation. Recently, a new APP processing pathway was reported by Willem et al.[6], in which sequential cleavage of APP by η-secretase and BACE1 or ADAM10 produces Aη-β and Aη-α, respectively. There may be other alternate processing of APP unidentified at this moment.

These observations show that the accumulation of Aβ species is governed by a biochemical network, in which there are multiple enzymes that may serve as a target to modify the exposure to distinct Aβ peptide species. The network structure complicates the prediction of the effect of inhibitors of the various enzymes on the exposure to the various Aβ species. This may explain the mixed observations in some of the early clinical trials with enzyme inhibitors. Against this background we have recently proposed a systems pharmacology model to describe the effect of BACE1 inhibition on multiple Aβ species[1].

Inhibitors of the two secretases that generate Aβ from APP, BACE1 and GS inhibitors, have been proposed as potential disease-modifying approaches in the treatment of AD[3]. Several BACE1 inhibitors are presently in clinical trials. The BACE1 inhibitor E2609 (Eisai) is currently in Phase II clinical development, MK-8931 (MSD) has advanced to Phase III and AZD 3293 (Eli Lilly and AstraZenica) recently progressed to Phase III. Various GS inhibitors, acting downstream on the APP pathway compared to BACE1 inhibitors, have also been pursued in the pharmaceutical industry. The GS inhibitor MK-0752 was progressed to Phase I, but then discontinued due to tolerability issues. The GS inhibitor avagecestat (BMS-708163) was discontinued after Phase II because of lack of efficacy and adverse effects of the gastrointestinal and dermatological system[7]. The

development of the GS inhibitor begacestat (GSI953) was discontinued after several Phase I trials. Begacestat reduced plasma Aβ40 levels but not CSF Aβ40[8]. The Phase III trial of the GS inhibitor semagacestat (LY450139) was terminated before completion, because semagacestat was associated with worsening of cognition and function, as well as adverse events such as skin cancers[9]. As yet, no GS inhibitor demonstrated therapeutic success in AD patients.

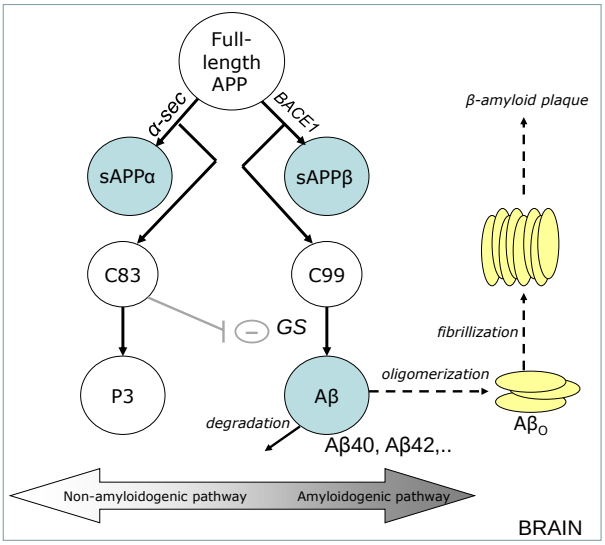

Figure 5.1: The amyloid hypothesis of AD.
In the APP processing pathway, full length APP is cleaved by β-secretase (β-sec) or α-secretase (α-sec) to form sAPPβ and C99 or sAPPα and C83. C99 is then cleaved by γ-secretase (γ-sec) to form Aβ. In a possible feedback loop C83 binds to GS γ-secretase leading to a reduction of Aβ (grey lines). The amyloid hypothesis states that an imbalance in production and clearance of Aβ can result in aggregation of Aβ42 fragments into amyloid plaque.

A better understanding of the drug-induced modulation of the APP system after GS inhibition, may be obtained through a quantitative comprehension of its concentration-response relationships. Several studies on the pharmacokinetics (PK) and the pharmacodynamics (PD) of GS inhibitors have been reported. Das et al. [10] reported a two-compartment model describing Aβ response to GS inhibition, as observed in plasma and CSF in rhesus monkeys. Their model postulates an inhibitory mechanism of Aβ clearance by GS inhibition. However, in their model aspects of the Aβ production, transport and clearance

processes were simplified. A model-based meta-analysis of published and in-house (pre-)clinical GS inhibitors data was performed by Niva et al. [11]. The production and clearance of Aβ was described with a turnover model, with a drug effect on the production rate. Tai et al. [12] also used turnover models to describe Aβ levels following GS inhibition in brain, CSF and plasma in wild type rat. They propose a quasi-static Aβ pool in the brain which does not change after short drug exposure.

The above mentioned approaches look solely at the behaviour of Aβ and not at the behaviour of the APP system as a whole. The understanding of the APP system is imperative to improve the prediction of drug effects on Aβ levels. Recently, a systems pharmacology model of the APP processing pathway was developed to characterize the APP metabolites responses to BACE1 inhibition by MBi-5 [1], distinct from MSD's BACE1 inhibitor MK-8931. Throughout the article the term 'recent model' is used to refer this model. The recent model took into account the kinetics and interrelationships of sAPPβ, sAPPα, Aβ40 and Aβ42. In the model, sAPPβ was used as a surrogate substrate for C99 in the γ-secretase cleavage step, modulating the responses of Aβ40 and Aβ42 in the presence of the BACE1 inhibitor. A precursor APP pool, shared by sAPPα and sAPPβ, was included to describe the effect on all four biomarkers with a single drug effect. The effect of BACE1 inhibition was built-in the model as inhibition of the pathway mediated by BACE1. Using this model, it was demonstrated that BACE1 inhibition resulted in a larger absolute reduction of CSF levels of Aβ40 than of Aβ42, as the effect on Aβ42 was modulated by back-conversion from an oligomer (Aβ_{O}) pool.

There is growing evidence that Aβ_{O} have a central role in the pathogenesis of AD [13]. Toxic Aβ_{O} are considered to be the drivers of neurodegeneration. Aβ_{O} might exist in a complex equilibrium with Aβ monomers and fibrils [14]. Treatments that prevent Aβ production may reduce the concentration of Aβ_{O} and subsequently promote the release of soluble Aβ from fibrils to restore the equilibrium [15].

The objective of the current investigation was to elucidate the APP processing pathway further, by challenging the recently developed systems pharmacology model of the APP pathway to describe Aβ dynamics following GS inhibition. The aims were (i) to separate β-secretase and γ-secretase sequential cleavage steps; (ii) to investigate possible differences in Aβ response following GS versus BACE1 inhibition; and (iii) to evaluate if moderation of Aβ42 by back-conversion from an Aβ_{O} pool could also be identified after inhibiting GS. To this end, CSF Aβ40 and Aβ42 response data from two studies of the GS inhibitor MK-0752 in cisterna magna ported rhesus monkeys [16] were analysed simultaneously with data from a BACE1 inhibitor (MBi-5) study, using the APP systems model.

Materials and Methods

Animals

All animal studies were reviewed and approved by the MSD Institutional Animal Care and Use Committee. The NIH Guide to the care and use of Laboratory Animals and the Animal Welfare act were followed in the conduct of the animal studies (Institute of Laboratory Animal Resources, National Research Council, 1996). The CMP rhesus monkey model was reported by Gilberto et al.[17]. The rhesus monkeys are chronically implanted with catheters in the cisterna magna, facilitating repeated sampling of CSF and plasma (through a jugular vascular access point). These rhesus monkeys were individually housed and captive-bred in a closed colony.

In the first GS inhibitor study (study 1), six male animals, weighing between 6.9 kg and 9.6 kg (mean, 8.2 kg), age n=5 at 5 years to 8 years (mean, 6 years) and 1 animal aged 17 years at time of study were included. The second GS inhibitor study (study 2) included six male animals, weighing between 6.1 kg and 12.3 kg (mean, 9.1 kg), age 7 to 10 years (mean, 8 years). In the BACE1 inhibitor study (study 3), six male animals, weighing between 5.2 kg and 11.7 kg (mean, 8.7 kg), age 2 to 10 years (mean, 8 years), were included. Half of the animals in the BACE1 inhibitor study participated also in the GS inhibitor studies.

Drug administration and sampling

The effects of secretase inhibition were obtained in three studies. In study 1, information on the effect of GS inhibition on Aβ40 and Aβ42 was obtained following a single oral administration of MK-0752 (3-((1r,4s)-4-(4-chlorophenylsulfonyl)-4-(2,5-difluorophenyl)cyclohexyl)propanoic acid) at 60 and 240 mg/kg (5 mL/kg) in a vehicle controlled (sterile water) three-period crossover study. In study 2, the effect of GS inhibition on Aβ40 and Aβ42 was measured during a follow-up collection period, following a single oral dose of MK-0752 at 240 mg/kg (5 mL/kg) in a vehicle controlled (sterile water) study. In study 3, the effect of BACE1 inhibition on sAPPα, sAPPβ, Aβ40 and Aβ42 were measured, following a single, oral administration of MBi-5 at 10, 30, 125 mg/kg (5 mL/kg), or vehicle (0.4% methylcellulose) in a four-way full crossover study. The study protocols of study 1 and 2 and pharmacological profile of MK-0752 were previously described by Cook et al.[16]. The detailed study protocol of study 3 and pharmacological profile of MBi-5 were described by Dobrowolska et al.[18]. The study protocols are summarized here.

In study 1, plasma and CSF drug concentrations were collected at 0 (predose) and 3, 5, 7, 9, 13, 16, 19, 22, 25, 28, 31, 34, 37, 40 and 49 h postdose, resulting in 16 plasma and CSF PK samples for each monkey per treatment. In study 2, plasma and CSF samples were collected as described for study 1 and additional samples were taken at 73, 145, 169, 217 and 241 h postdose, resulting in 21 plasma and CSF PK samples for each monkey. 2 mL of blood and 1 mL of CSF were collected at each time point. The concentration of MK-0752 in the plasma and CSF samples was determined using LC-MS/MS. The concentrations of Aβ40 and Aβ42 were determined from CSF samples collected at the same time points as PK samples, giving 16 measurements of each biomarker for each monkey per treatment in study 1 and 21 measurements of each biomarker for each monkey in study 2. The Aβ1-40 and Aβ1-42 assays used for the concentration measurements were described previously by Cook et al. [16].

In study 3, plasma and CSF drug concentrations were collected at 0 (predose) and 3, 5, 7, 9, 13, 16, 19, 22, 25, 28, 31, 49, 55, 58, 73 and 145 h postdose, resulting in 17 plasma and CSF PK samples for each monkey per treatment group. 2 mL of blood and 1 mL of CSF were collected at each time point. The concentration of MBi-5 in the plasma and CSF samples was determined using LC-MS/MS. The concentrations of Aβ40, Aβ42, sAPPα and sAPPβ were determined from CSF samples collected at -22, -20 and -1h (predose) and 2, 4, 6, 8, 12, 15, 18, 21, 24, 27, 30, 48, 54, 57, 72 and 144 h postdose, giving 19 measurements of each biomarker for each monkey per treatment group. 1 mL of CSF were collected at each time point. The specific enzyme-linked immunosorbent assays used for the concentration measurements were described previously [19,20].

PK-PD analysis

PK-PD modelling analysis was performed by means of non-linear mixed effects modelling using the software package NONMEM (version 7.2.0 [21]). In this approach, structural (fixed) effects and both intra- and interindividual variability are taken into account. Typical values of structural model parameters (population parameters, which define the average value for a parameter in a population) (θ), the variance and covariance of the interindividual variability (ω^2) and the variance of the residual error (σ^2) are estimated.

The best models were chosen based on minimum value of the objective function, the precision of parameter estimates, and visual inspection of goodness-of-fit plots. A more detailed description of the modelling procedure was described in van Maanen et al. [1].

To evaluate the performance of the model a visual predictive check (VPC) was performed in which the median and the 90% inter-quantile range of the data simulated

with the final parameter estimates were overlayed with the observations. The predictive capacity is considered sufficient when the median and 90% of predictions line up within the 5th, 50th and 95th percentiles of the observations.

The NONMEM software package was implemented on an Intel QuadCore (Intel®Core^{TM} i7 CPU860, 2.80 GHz, 3.24 GB RAM) and Compaq Visual Fortran (version 6.6, Compaq Computer Corporation, Houston, Texas, USA) was used as compiler. Data management and model assessment was done using the statistical software package S-PLUS for Windows (version 8.0 Professional, Insightful Corp., Seattle, USA).

Model description

The systems model of the APP processing pathway was developed by sequential analysis of PK and PD data following administration of MBi-5 and MK-0752. The PK models of MBi-5 and MK-0752 were based on simultaneous analysis of plasma and CSF PK data of each compound. The results of the PK data analysis of MBi-5 have been reported elsewhere by van Maanen et al.[1]. The results of the PK data analysis of MK-0752 are reported in the supplemental material.

The PK models adequately described the plasma and CSF concentration time profiles of MBi-5 and MK-0752, respectively, thus the models could serve as input for PD model analysis.

The interrelationships of APP metabolite responses to BACE1 inhibition were described recently using a comprehensive systems model of the APP processing pathway[1]. To describe the effect of the GS inhibitor, the model had to be extended.

The extended systems model of the APP processing pathway included a compartment for C99. The relation between Aβ and C99 was included in the model, representing the γ-secretase cleavage step, on which the drug effect of MK-0752 was implemented. In addition, sAPPβ was no longer used as driver of Aβ response and a sAPPβ elimination path was incorporated into the model.

The biomarker response profiles of MBi-5 and MK-0752 measured in CSF were adequately described by a model containing compartments for seven moieties: APP, sAPPβ, sAPPα, C99, Aβ40, Aβ42 and Aβ_{O} (Fig. S5.1). The production of APP was assumed to be constant and described by a zero order input rate constant Rin_{APP}. The production of the APP metabolites was assumed to be first order, i.e. dependent on its precursor concentration. The relationship between APP and its metabolites (sAPPβ, sAPPα, C99, Aβ40 and Aβ42) and Aβ_{O} is described by Eq. 5.1 - Eq. 5.7:

$$\frac{d}{dt}APP = Rin_{APP} - (Rin * EFFB + Rin_2) * APP \tag{5.1}$$

$$\frac{d}{dt}sAPP\alpha = Rin_2 * APP - Rout_a * sAPP\alpha \tag{5.2}$$

$$\frac{d}{dt}sAPP\beta = Rin * EFFB * APP - Rout_b * sAPP\beta \tag{5.3}$$

$$\begin{aligned}\frac{d}{dt}C99 =& Rin * EFFB * APP - (Kin_{40} + Kin_{42}) * EFFG * C99 \\ & - Kout_{99} * C99\end{aligned} \tag{5.4}$$

$$\frac{d}{dt}A\beta_{40} = Kin_{40} * EFFG * C99 - Kout * A\beta_{40} \tag{5.5}$$

$$\begin{aligned}\frac{d}{dt}A\beta_{42} =& Kin_{42} * EFFG * C99 - Kout * A\beta_{42} - Kpl \times A\beta_{42} \\ & + Krev \times A\beta_O\end{aligned} \tag{5.6}$$

$$\frac{d}{dt}A\beta_O = Kpl \times A\beta_{42} - Krev \times A\beta_O \tag{5.7}$$

The rate of change of APP with respect to time in the presence of the BACE1 inhibitor is expressed by Eq. 5.1, in which the BACE1 cleavage inhibition is incorporated by the factor *EFFB*. The rate of change of C99 with respect to time in the presence of the GS inhibitor is described by Eq. 5.4, in which the GS cleavage inhibition is incorporated by the factor *EFFG*. *EFFB* and *EFFG* are the degrees of inhibition caused by MBi-5 and MK-0752, respectively. Generally, the degree of inhibition is described by a sigmoidal Imax function, as shown in Eq. 5.8.

$$EFF = 1 - \frac{C_{target}^{GAM} * Imax}{C_{target}^{GAM} + IC50^{GAM}} \tag{5.8}$$

Where C_{target} is the target site concentration of MBi-5 or MK-0752, respectively, *IC50* the C_{target} that results in 50% inhibition of BACE1 or GS, *Imax* is the maximum response and *GAM* is the Hill coefficient. C_{target} was derived from the respective PK models as:

$$C_{target} = C_{plasma} * \frac{AUC_{CSF}}{AUC_{plasma}} \tag{5.9}$$

Where AUC_{CSF} and AUC_{plasma} are the areas under the CSF and plasma concentration time curves, respectively. C_{target} is assumed to be in steady state with C_{plasma}.
It is assumed that the system is in steady state (SS) when no treatment is given *(EFFB=1, EFFG=1)*. These steady state conditions were used to derive part of the system parameters. From SS and Eq. 5.1 it follows that the zero order input rate constant of APP *(Rin_{APP})* is:

$$Rin_{APP} = (Rin_{\alpha} + Rin_{\beta}) * APP_{base} \tag{5.10}$$

Where APP_{base} is the baseline level of APP, assumed to be equal to the sum of the baseline levels of sAPPα and sAPPβ. All alternate pathways are represented by the terms for α-secretase.
Using SS conditions and Eq. 5.2 the sAPPα formation rate constant (Rin_{α}), equivalent to the α-secretase cleavage step, can be derived:

$$Rin_{\alpha} = Rout_a * \frac{sAPP\alpha_{base}}{APP_{base}} \tag{5.11}$$

Where sAPPα_{base} is the baseline level of sAPPα.
The sAPPβ and C99 formation rate constant (Rin_{β}), equivalent to the BACE1 cleavage step, follows from SS conditions and Eq. 5.3:

$$Rin_{\beta} = Rout_b * \frac{sAPP\beta_{base}}{APP_{base}} \tag{5.12}$$

Where $sAPP\beta_{base}$ is the baseline level of sAPPβ.

From Eq. 5.5 and SS, the Aβ degradation rate constant (*Kout*), is deduced:

$$Kout = Kin_{40} * \frac{C99_{base}}{A\beta 40_{base}} \tag{5.13}$$

Where *C99*$_{base}$ is the baseline level of C99. Please not that C99 is not an observed measure. From Eq. 5.4 and SS the baseline level of C99 can be calculated:

$$C99_{base} = \frac{Rout_b * sAPP\beta_{base}}{Kin_{40} + Kin_{42} + Kout_{99}} \tag{5.14}$$

Combining Eq. 5.13 and Eq. 5.14, the Aβ42 formation rate constant (*Kin42*), equivalent to a GS cleavage step, can be written as:

$$Kin_{42} = Kout * \frac{A\beta 42_{base}}{A\beta 40_{base}} \tag{5.15}$$

Kpl and *Krev* are the Aβ42 oligomerization and dissociation rate constant, respectively, which are dependent on the baseline values of Aβ42 and the Aβ_{O} pool (A$\beta 42_{base}$ and Aβ_{Obase}, resp.) according to Eq. 5.16:

$$Krev = \frac{Kpl \times A\beta_{42base}}{A\beta_{Obase}} \tag{5.16}$$

The model structure includes four transit compartments (Fig. S5.1), one for each biomarker measured in CSF (sAPPα, sAPPβ, Aβ40, Aβ42), to account for transport from the target site in the brain to CSF. These transit processes are described, in general, by Eq. 5.17:

$$\frac{d}{dt} xAx_{CSF} = Ktr * (xAx - xAx_{CSF}) \tag{5.17}$$

Where *Ktr* is the transit rate constant for the particular APP metabolite xAx (sAPPα, sAPPβ, Aβ40, Aβ42).

Results

Aβ response to GS and BACE1 inhibition was described by separate descriptive models

Initially, empirical PK-PD models were developed to quantify the exposure-response relationships for each CSF APP metabolite of the BACE1 inhibitor MBi-5 (Aβ40, Aβ42, sAPPα and sAPPβ) and GS inhibitor MK-0752 (Aβ40 and Aβ42) in rhesus monkeys. For the BACE1 inhibitor MBi-5, the empirical PK-PD models for Aβ40, Aβ42, sAPPα and sAPPβ were discussed recently in van Maanen et al.[1]. For MBi-5 and MK-0752, we now present the empirical PK-PD models for Aβ40 and Aβ42. The exposure-response relationship for each Aβ-inhibitor combination was described by a transit model with 1 or 2 compartments, with the drug effect modelled relative or subtractive to baseline using an Imax function. Table 5.1 presents a summary overview of the results of these models. For each inhibitor, the empirical models identified similar drug effects for Aβ40 and Aβ42: for MBi-5 the identified potencies were Aβ40: 0.0254 μM (95% CI, 0.0246-0.0262) and Aβ42: 0.0455 μM (95% CI, 0.0351-0.0559) and for MK-0752 the identified potencies were Aβ40: 0.432 μM (95% CI, 0.300-0.564) and Aβ42: 0.567 μM (95% CI, 0.402-0.732).

The separate empirical models revealed potential challenges for the combined analysis. Firstly, there are study differences in Aβ baselines: Aβ40 baseline is 1.5 fold higher and the Aβ42 baseline is 3.4 fold higher in the GS inhibitor studies (study 1 and 2) compared to the BACE1 inhibitor study (study 3). Consequently, the ratio of Aβ42:Aβ40 is higher in the GS inhibitor studies: 0.078 for the GS inhibitor studies and 0.034 for the BACE1 inhibitor study, respectively. Secondly, the mean transit time through the compartments of the models was lower for Aβ42 after BACE1 inhibition than Aβ42 after GS inhibition. This indicated that the response of Aβ42 to BACE1 inhibitor will appear earlier in CSF than with GS inhibition. Sequentially, BACE1 inhibition interferes earlier in the amyloidogenic APP pathway. This suggested a temporal difference in relative response progression of Aβ42 following BACE1 *versus* GS inhibition. For Aβ40, the mean transit time was higher after BACE1 inhibition than after GS inhibition, however overlapping confidence intervals suggest insignificant differences.

A systems model to describe APP metabolite responses to GS and BACE1 inhibition

Recently, we reported a systems pharmacology model, incorporating the pharmacokinetics of MBi-5 and APP metabolites (Aβ40, Aβ42, sAPPβ and sAPPα) concentrations[1]. In

Table 5.1: Summary parameters of the separate empiric model fits for Aβ40 and Aβ42 for each inhibitor

PARAMETER	DESCRIPTION	UNIT	MBi-5		MK-0752	
			Aβ40	Aβ42	Aβ40	Aβ42
baseline	baseline	pM	722	24.8	1080	83.3
Imax	maximal inhibition		100%[a,b]	20.4 pM [c]	100%[a]	100%[a]
IC_{50}	median inhibition concentration	μM	0.0254	0.0455	0.432	0.567
			(*CV*	(*CV*	(*CV*	(*CV*
			1.63%)	*11.6%*)	*15.6%*)	*14.8%*)
GAM	Hill coefficient		1[a]	1[a]	1.70	1.48
MTT[d]	Mean transit time (MTT)	h	5.155	3.597	4.651	5.435
	95% confidence interval MTT	h	(4.23-6.60)	(2.42-7.08)	(3.72-6.21)	(4.26-7.52)

[a] Fixed.

[b] $Effect = baseline * (1 - \frac{C_{target}^{GAM} * Imax}{C_{target}^{GAM} + IC_{50}^{GAM}})$

[c] $Effect = baseline - \frac{C_{target}^{GAM} * Imax}{C_{target}^{GAM} + IC_{50}^{GAM}}$

[d] $MTT = \frac{1}{Kt} \times (n+1)$, where *n* is the number of transit compartments and *Kt* is the transit rate.

the current analysis, the model was extended to describe dynamics of Aβ responses after exposure to a GS inhibitor. To this end, the APP metabolite responses of Aβ40, Aβ42, sAPPβ and sAPPα following BACE1 inhibition and Aβ40 and Aβ42 response following GS inhibition were analysed simultaneously.

To closer match the APP processing pathway, a C99 compartment was added to the model structure. As sAPPβ and C99 are both products of the same BACE1 cleavage step, the formation rate constant of C99 was set to be equal to the formation rate constant of sAPPβ (*Rin*β). The effect of BACE1 inhibition was incorporated in the model as inhibition of *Rin*β. The effect of GS inhibition was modelled as inhibition of the Aβ40 and Aβ42 formation rate out off the C99 compartment, consistent with the γ-secretase cleavage step. The elimination of sAPPβ (*RoutB*) could now be described as a separate parameter.

Inclusion of a C99 compartment and the estimated GS inhibition rates implied rebound of Aβ40 and Aβ42 response after GS inhibition: Simulations indicated an excessive response above baseline upon cessation of GS inhibition (not shown). However, the data did not suggest any significant rebound. Therefore, the model was refined by adding an alternative elimination pathway of C99 (*Kout99*) and hence preventing rebound. The resulting model structure is presented in Figure 5.2.

Inter-study baseline differences were evaluated by adding baseline data from two other studies (Study A and B) (see Supplemental Material). From this, it became apparent that a correction for Aβ baseline differences between studies needed to be included. The

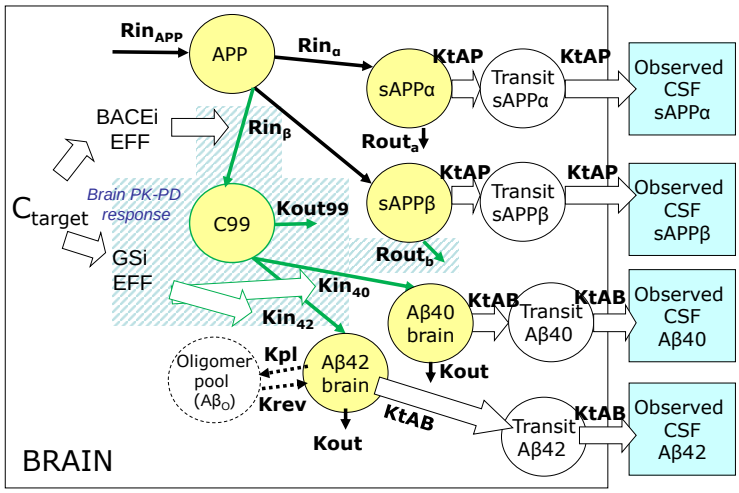

Figure 5.2: Schematic of model structure.
The model comprised eleven compartments: Six biomarker compartments in brain *(yellow)*, one oligomer pool *(blank dashed)* and four transit compartments from brain to CSF *(blank)*. Four biomarkers were measured in CSF (sAPPα, sAPPβ, Aβ40 and Aβ42), indicated by the blue boxes. The model included a C99 compartment *(dashed)*, which was not present in the model based on β-secretase inhibition data only. Model extensions are indicated with the green shaded area. The drug effect of the β-secretase inhibitor *(BACEi EFF)* inhibited *Rin*. The drug effect of the γ-secretase inhibitor *(GSi EFF)* inhibited Kin_{42} and Kin_{40}. As driver of biomarker response C_{target} was used, which was derived from the respective PK models (not shown).
APP: Aβ-precursor protein; *A*β: amyloid-β-peptide; C_{target}: drug concentration target site; Kin_{40}: Aβ40 formation rate; Kin_{42}: Aβ42 formation rate; *Kout*: Aβ degradation rate; $Kout_{99}$: C99 degradation rate; *KtAP*: transit rate sAPPα and sAPPβ from brain to CSF; *KtAB*: transit rate Aβ from brain to CSF; *RinAPP*: source of APP; *Rin*α: sAPPα formation rate; *Rin*β: sAPPβ and C99 formation rate; *Routa*: sAPPα degradation rate; *Routb*: sAPPβ degradation rate. *Kpl*: Oligomerization rate; *Krev*: $A\beta_O$ dissociation rate.

underlying biological system was assumed to be the same during all studies. Therefore, scaling factors were included on the model predictions (IPRED) for Aβ40 and Aβ42 outside of the system. To improve the model description further, differences in parameter values following BACE1 or GS inhibition were investigated. The formation rate constant of Aβ40 (*Kin40*) was fixed to the value identified recently (0.574 h^{-1}) following BACE1 inhibition[1] and a significantly lower *Kin40* was identified after GS inhibition (0.349 h^{-1} (95% CI: 0.296-0.402). Also, a substantial reduction of the Aβ42 oligomerization rate constant (*Kpl*) after GS inhibition was found (95% reduction). Including these differences improved the description of all the biomarkers.

Overall, the data were adequately captured across studies (Fig.5.3-5.6). Only a slight

underprediction was observed for the baseline level of Aβ40 in study 1 (Fig. 5.3A) and the maximal Aβ42 response to 240 mg/kg MK-0752 (Fig. 5.5B and 5.5C) and 125 mg/kg MBi-5 (Fig. 5.5F).

The model separated drug-specific and system-specific parameters

The population parameters and intra- and interanimal variability were optimized for the all study populations simultaneously and are reported in Table 5.2. Interanimal variability was included as exponential in nature, reflecting lognormal distributions of the individual model parameters, for the baseline of sAPPβ, the IC50 of MBi-5 and the IC50 of MK-0752. As the baselines of other APP metabolites were modelled as function of the baseline of sAPPβ, the interanimal variability of sAPPβ is propagated in these biomarkers. Residual variability was included for each APP

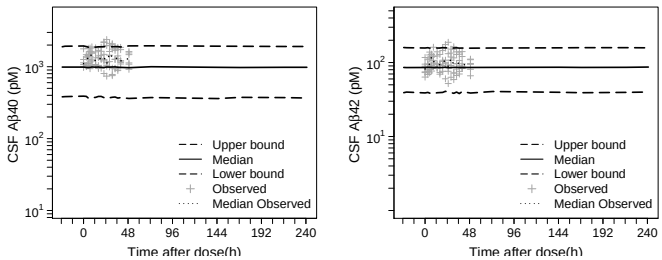

(A) Aβ40 placebo St1 ***(B) Aβ42 placebo St1***

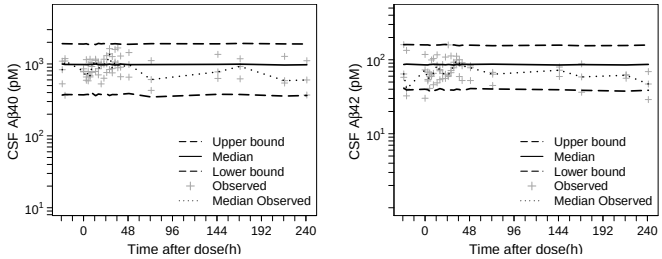

(C) Aβ40 placebo St2 ***(D) Aβ42 placebo St2***

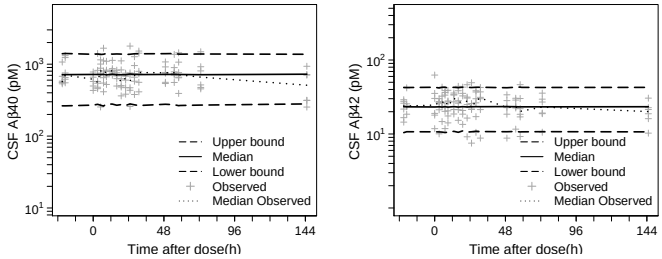

(E) Aβ40 placebo St3 ***(F) Aβ42 placebo St3***

Figure 5.3: Placebo. Aβ. Simulations of biomarker response* vs. *time profile of placebo in the rhesus with 90% confidence interval. Observation sample size: n=114 for each APP metabolite from 6 monkeys collected over 7 days. *Solid line:* Median predicted. *Long-dashed line:* 90% prediction interval. *Dotted line:* Median observed. + *symbol:* Observations.

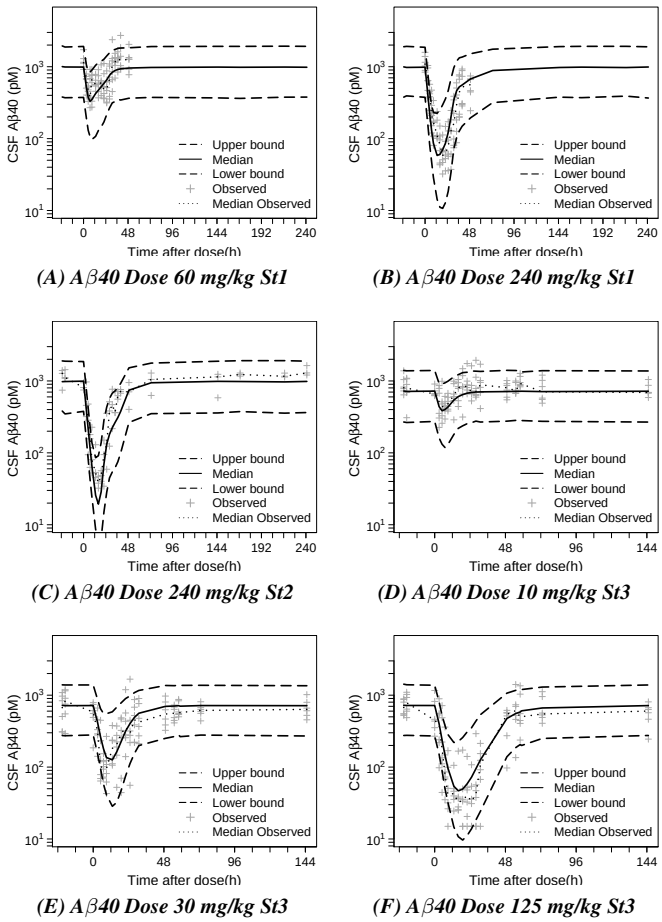

(A) Aβ40 Dose 60 mg/kg St1 *(B) Aβ40 Dose 240 mg/kg St1*

(C) Aβ40 Dose 240 mg/kg St2 *(D) Aβ40 Dose 10 mg/kg St3*

(E) Aβ40 Dose 30 mg/kg St3 *(F) Aβ40 Dose 125 mg/kg St3*

Figure 5.4: Aβ40. Simulations of biomarker response* vs. *time profile of Aβ40 in the rhesus with 90% confidence interval. Observation sample size: n=114 for each APP metabolite from 6 monkeys collected over 7 days. *Solid line:* Median predicted. *Long-dashed line:* 90% prediction interval. *Dotted line:* Median observed. + *symbol:* Observations.

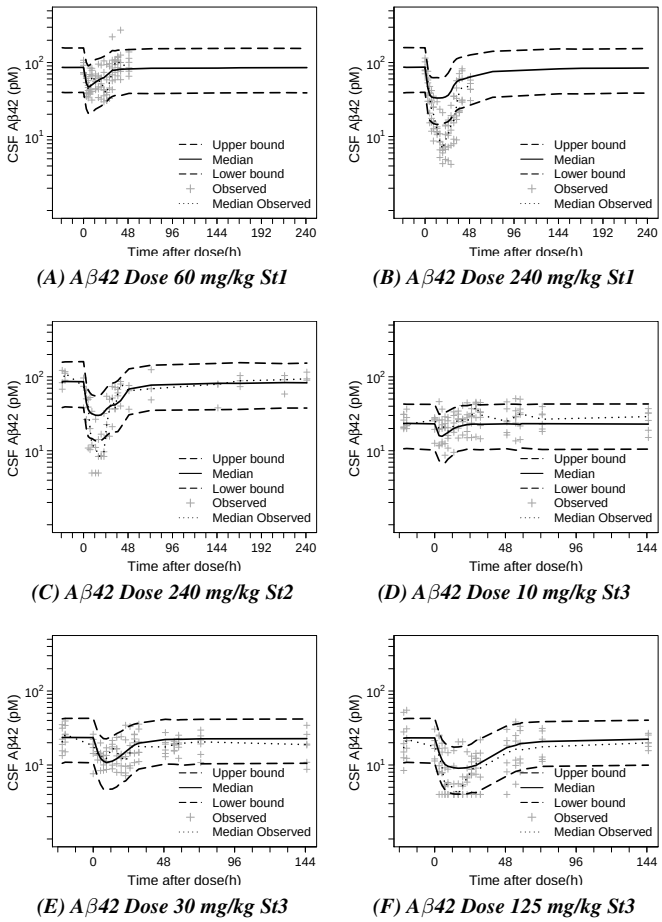

Figure 5.5: Aβ42. Simulations of biomarker response* vs. *time profile of Aβ42 in the rhesus with 90% confidence interval. Observation sample size: n=114 for each APP metabolite from 6 monkeys collected over 7 days. *Solid line:* Median predicted. *Long-dashed line:* 90% prediction interval. *Dotted line:* Median observed. + *symbol:* Observations.

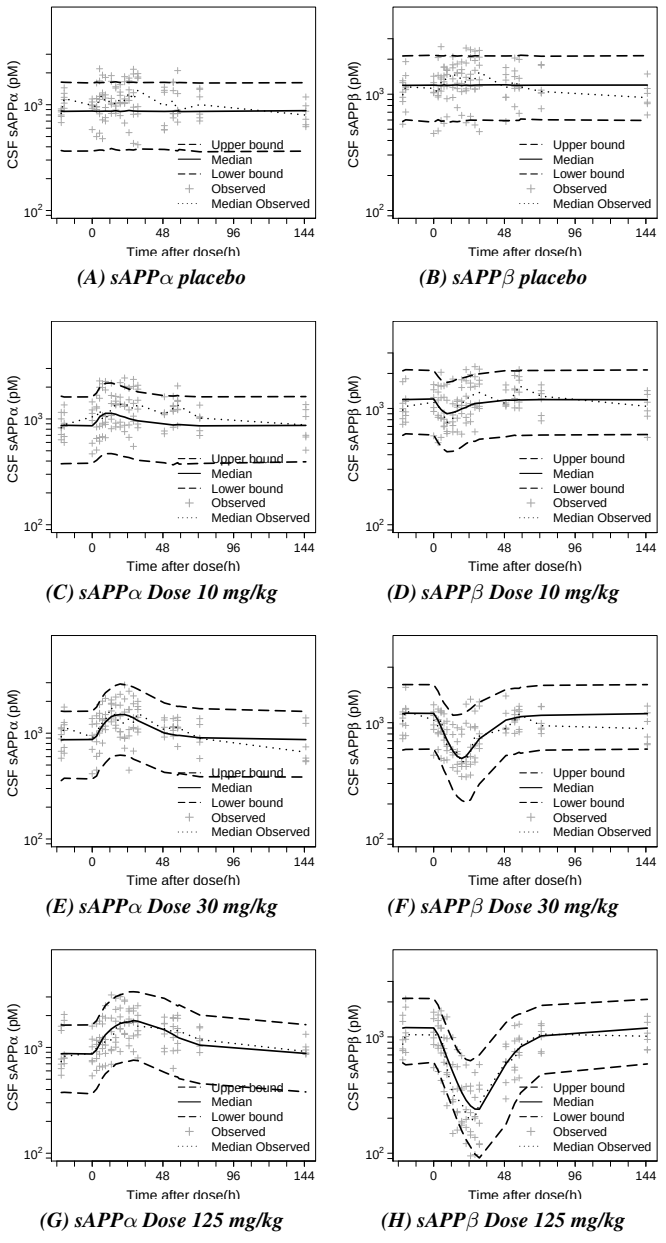

Figure 5.6: sAPPα* (left) *and sAPPβ (*right*). Simulations of biomarker response* vs. *time profile of MBi-5 in the rhesus with 90% confidence interval. Observation sample size: n=114 for each APP metabolite from 6 monkeys collected over 7 days. *Solid line:* Median predicted. *Long-dashed line:* 90% prediction interval. *Dotted line:* Median observed. + *symbol:* Observations.

metabolite (sAPPβ, sAPPα, Aβ40, Aβ42), as proportional error models, assuming a normal distribution. Drug specific parameters (*IC50, GAM, IM*) could be distinguished from system specific parameters (Kin_{40}, $Kout_{99}$, $Rout_a$ $Rout_b$, *KtrAP, Kpl, Krev*). The correlations between parameters were all below 0.95.

The transit rate constant from brain-to-CSF for Aβ40 and Aβ42 was assumed to be equal and fast. As the transit rate for sAPPβ and sAPPα can only be estimated relative to the transit rate of Aβ, the latter was fixed to an arbitrary high value (10 h^{-1}). The transit rate constant for sAPPβ and sAPPα was estimated to be 0.0847 h^{-1}, which should be interpreted relative to the Aβ transit rate constant.

Correction factors on Aβ42 and Aβ40 for study differences in levels compared to study 3 were 3.7 (95% CI, 3.40-4.00) and 1.37 (95% CI, 1.26-1.48), which were imputed as multipliers on the respective IPREDs of Aβ42 and Aβ40.

The IC_{50} of MBi-5 was estimated to be 0.0185 μM (95% CI, 0.0149-0.0221); the IC_{50} of MK-0752 was 0.445 μM (95% CI, 0.337-0.553). The Hill coefficients for both compounds slightly deviated from unity: MBi-5 1.49 (95% CI, 1.35-1.63) and MK-0752 1.73 (95% CI, 1.54-1.92).

Differences in APP metabolite interrelationships following BACE1 and GS inhibition

The formation rate constant of Aβ42 (Kin_{42}) was calculated according to Equation 5.15: 0.0186 h^{-1} and 0.0113 h^{-1} in the BACE1 and GS inhibition studies, respectively. Kin_{42} was higher than the formation rate constant of Aβ40 (Kin_{40}: 0.574 h^{-1} and 0.349 h^{-1}, in the BACE1 and GS inhibition studies, respectively). This is in agreement with the previously reported ratio of Aβ42 and Aβ40 of about 1:10 in non-Alzheimer brain (Iwatsubo et al. [22]).

The resulting model was used to visualize the interrelationships of the biomarkers following BACE1 and GS inhibition, respectively. Also, the behaviour of APP, C99 and $A\beta_O$ was predicted. The relationships of the biomarker responses to BACE1 inhibition were recently discussed in van Maanen et al. [1]. The differentiation in biomarker response to inhibition of BACE1 and GS was as followed. APP increases after BACE1 but not after GS inhibition (Figure 5.7A and 5.7B, respectively). C99 decreases following BACE1 inhibition and slightly increases following GS inhibition. Both BACE1 and GS inhibition are predicted to decrease $A\beta_O$ levels, implying that the formation of $A\beta_O$ is reduced by decreased levels of monomeric Aβ42 and that $A\beta_O$ is in dynamic equilibrium with monomeric Aβ42.

Table 5.2: Population parameter estimates including coefficient of variation (CV%)

PARAMETER	DESCRIPTION	VALUE	UNIT	CV%
Structural parameters				
sAPPβ_{base}	baseline sAPPβ	1.22e+3	pM	4.44
Fbase$^{b}_{A\beta 40}$	Aβ40 baseline as fraction of sAPPβ_{base}	0.602		2.56
Fbase$^{c}_{A\beta 42}$	Aβ42 baseline as fraction of sAPPβ_{base}	0.0195		2.37
Fbase$^{d}_{sAPP\alpha}$	sAPPα baseline as fraction of sAPPβ_{base}	0.729		2.15
Kin$_{40}$B^{a}	formation rate Aβ40 following BACE1 inhibition *(fixed)*	0.574	h^{-1}	
Kin$_{40}$G	formation rate Aβ40 following GS inhibition	0.349	h^{-1}	7.68
Kout$_{99}$	degradation rate C99	4.70	h^{-1}	10.1
Rout$_{a}$	degradation rate sAPPα	1.80	h^{-1}	13.3
Rout$_{b}$	degradation rate sAPPβ	1.79	h^{-1}	9.61
KtrAP	transit rate sAPPα and sAPPβ	0.0847	h^{-1}	4.17
KtrAB^{a}	transit rate Aβ*(fixed)*	10	h^{-1}	
IMB^{a}	Imax BACE *(fixed)*	1		
IC50B	IC50 BACE	0.0185	μM	9.89
GAMB^{a}	Hill coefficient	1.49		4.72
IMG^{a}	Imax GSi *(fixed)*	1		
IC50G	IC50 GSi	0.445	μM	12.4
GAMG^{a}	Hill coefficient	1.73		5.55
KplB	oligomerization rate following BACE1 inhibition	0.183	h^{-1}	13.3
FKplG^{e}	factor on oligomerization rate following GS inhibition	0.0512		21.3
Krev	oligomer dissociation rate	0.0104	h^{-1}	64.7
FAC1	correction factor for study differences Aβ42	3.70		4.16
FAC2	correction factor for study differences Aβ40	1.37		4.25
Interanimal variability				
ω^2_{BSAPb}	Interanimal variability sAPPβ baseline	0.0672		20.4
ω^2_{IC50B}	Interanimal variability IC50 BACE	0.280		39.6
ω^2_{IC50G}	Interanimal variability IC50 GSi	0.176		44.8
Residual error				
$\sigma^2_{A\beta 40}$	Residual variability Aβ40	0.135		5.45
$\sigma^2_{A\beta 42}$	Residual variability Aβ42	0.0911		4.97
$\sigma^2_{sAPP\beta}$	Residual variability sAPPβ	0.0732		8.09
$\sigma^2_{sAPP\alpha}$	Residual variability sAPPα	0.106		8.53

[a] Fixed.

[b] A$\beta 40_{base}$=Fbase$_{A\beta 40}$*sAPPβ_{base}.

[c] A$\beta 42_{base}$=Fbase$_{A\beta 42}$*sAPPβ_{base}.

[d] sAPPα_{base}=Fbase$_{sAPP\alpha}$*sAPPβ_{base}.

[e] KplG=KplB*FKplG.

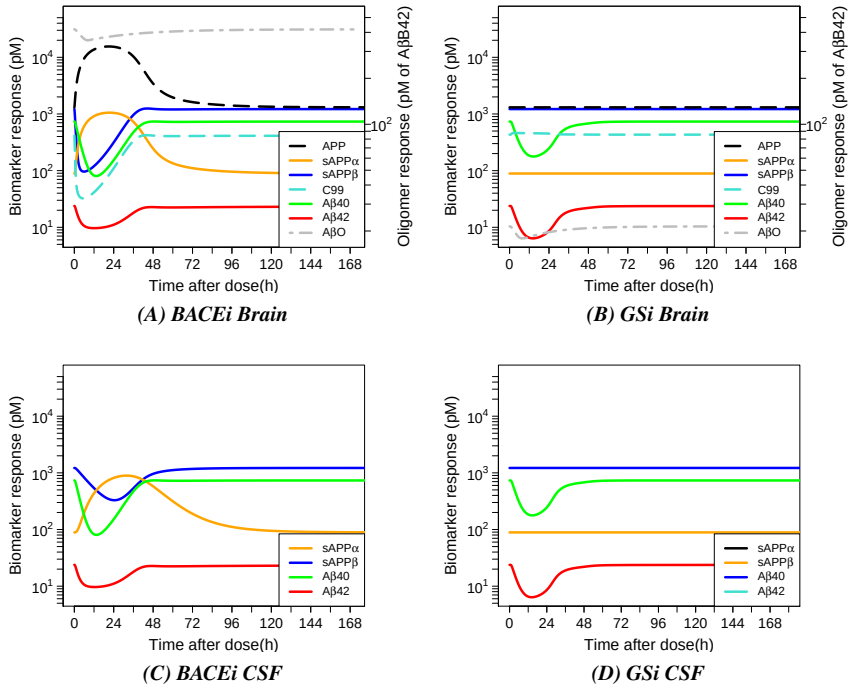

Figure 5.7: Simulation biomarker responses.
The biomarker responses are simulated after a single dose of 125 mg MBi-5 (A) (C) and single dose of 60 mg MK-0752 (B) (D).
APP black dashed line; *sAPP*α yellow solid line; *sAPP*β blue solid line; *C99* light blue dashed line; *A*β*40* green solid line; *A*β*42* red solid line; *A*β_{O} grey twodash line.

The simulated concentration of Aβ_{O} should be interpreted as the level if Aβ42 monomers tied in the 'oligomer soup' in the brain. The Aβ_{O} pool was modelled as a pool in equilibrium with monomeric Aβ42 without adaptation for the number of subunits in multimeric species contained in the Aβ_{O} pool. The simulated difference in Aβ_{O} concentration in Figure 5.7A and 5.7B therefore reflects a difference in the the number of monomers incorporated in the Aβ_{O} pool.

Discussion

A recently reported systems model of the APP processing pathway was extended to describe the interrelationships of Aβ40, Aβ42, sAPPβ, and sAPPα upon inhibition of BACE1 with MBi-5 and Aβ40 and Aβ42 upon inhibition of GS with MK-0752 simultaneously[1]. BACE1 acts earlier in the cascade, affecting all four biomarkers. Sequentially, GS inhibition interferes later in the amyloidogenic APP pathway and affects Aβ40 and Aβ42 only. In the recent model, sAPPβ was used as a surrogate substrate for C99 in the γ-secretase cleavage step, driving the response of Aβ. Consequently, the γ-secretase cleavage step could not be differentiated from sAPPβ elimination. Here, the combined model based analysis of BACE1 inhibitor and GS inhibitor response data facilitated the separation of the γ-secretase cleavage step from other processes involved. To that end, the extended systems model of the APP processing pathway included a compartment for C99, wherein the relationship between C99 and Aβ represents the γ-secretase cleavage step. As a result of this model extension, it was possible to identify the brain-turnover of sAPPβ as a separate parameter. Thus, the brain turnover of sAPPβ (0.39 hours) could be distinguished from the half-life of the brain-to-CSF transfer (8.2 hours).

Using the sAPPβ pool as moderator of Aβ in the recent model was a simplification of the underlying biological system. Here, the systems model structure more closely resembles the underlying APP pathway and the incorporation of the data following GS inhibition was essential for this.

The MK-0752 concentration dependent decrease of Aβ40 and Aβ42 could be described by incorporating a single drug effect in the model: inhibition of the formation rates of Aβ40 and Aβ42 out of the C99 compartment, equivalent to the GS cleavage step. The effect of BACE1 inhibition was incorporated in the model as inhibition of the formation of sAPPβ and C99 (*Rin*β), corresponding to the BACE1 cleavage step.

The elimination rate was higher for C99 than for sAPPβ. sAPPβ and C99 could be subjected to different elimination processes, conceivably because C99 remains membrane bound as opposed to sAPPβ, or has other biochemical/biophysical properties. The elimination rate of sAPPβ and sAPPα had similar values. Both are soluble fragments of APP, with overlapping sequence only differentiating in the 16 C-terminal amino-acids. The functions that are related to the shared domains of sAPPα and sAPPβ are identical (Chasseigneaux2012a). Therefore, it is not unlikely that sAPPα and sAPPβ also have similar elimination pathways.

The identified IC_{50} of MK-0752 in the empirical models were consistent with the

single potency identified using the systems model. Aβ is the product of GS cleavage of C99 and therefore Aβ response measurement following GS inhibition provides a direct reflection of the drug action. Hence, the IC50 values based on empirical *versus* the mechanistic systems model were similar for MK-0752. The estimated IC_{50} of MK-0752 (0.445 μM) is also similar to the brain IC_{50} in guinea-pigs of 440 nM [16].

For MBi-5, the identified IC_{50} in the empirical models were significantly higher than the single potency of 0.0185 μM identified using the systems model. As MBi-5 interferes earlier in the amyloidogenic APP pathway, inhibiting the formation of the Aβ precursor C99, Aβ response does not directly reflect the drug action. A systems model that includes key processes such as the production, elimination, and brain-to-CSF transport for the APP metabolites can more accurately describe the IC50 than an empirical model.

The identified IC_{50} of MBi-5 in the current analysis was lower 0.0185 μM (95% CI, 0.0149-0.0221) than recently identified 0.0269 μM (95% CI, 0.0154-0.0384) [1], however, confidence intervals overlap. The more complete systems model presented here, explains more fully the processes occurring in the APP pathway and therefore provides a more accurate characterization of IC50.

A significant difference in Aβ40 formation rate constant was identified following BACE1 and GS inhibition. This may reflect that the implementation of the GS cleavage step in the model is a simplification of the underlying system. Matsumura et al. [23] report multiple interactive pathways for stepwise successive processing of C99 by GS, which are hypothesized to define the Aβ isoforms and quantity of each Aβ. If Aβ40 and Aβ42 are indeed the products of consecutive GS cleavage, this may be reflected in the identified divergence in Aβ dynamics following GS inhibition *versus* BACE1 inhibition.

An alternative explanation of the differentiation in Aβ dynamics following BACE1 and GS inhibition may be that a feedback mechanism was activated. Tian et al. [24] propose that α-secretase cleavage initiates a feedback mechanism in which increased C83 may negatively modulate GS activity, thereby lowering Aβ production. As sAPPα and C83 are products of the same cleavage step by α-secretase, C83 will increase in a similar manner as sAPPα following BACE1 inhibition. The model predicts that C83 concentrations increase as result of BACE1 inhibition, but do not increase as result of GS inhibition. Therefore, we would expect this inhibitory effect on GS through C83 to occur after BACE1 inhibition, but not after GS inhibition. And this would then have to be reflected in a lower Aβ formation rate constant following BACE1 inhibition. However, a higher Aβ formation rate was found. The feedback mechanism as proposed by Tian was evaluated in the current model, but was not supported by the data.

It has been demonstrated that increased sAPPα generation is accompanied by a reduction of both β-secretase cleavage and Aβ generation [25]. The model predicts that C99 will decrease following BACE1 inhibition and slightly increases following GS inhibition. Increased C99 levels may have a stimulating effect on α-secretase. Stimulation of α-secretase will lead to enhanced production of sAPPα and C83 and reduced production of sAPPβ and C99 and, consequently, less Aβ being formed. This may be reflected in the lower Aβ formation rate constant that was identified following GS inhibition. As both sAPPα and sAPPβ levels following GS inhibition were not measured in the current study, the proposed mechanism cannot be confirmed using the current data, and will be investigated further in a follow-up study.

The interpretation of the Aβ_{O} pool was recently discussed in van Maanen et al. [1]. The systems analysis suggests a difference in oligomerization of Aβ42 after GS and BACE1. However, the maximal Aβ42 response to the higher dose groups of MBi-5 and MK-0752 were not adequately captured. Therefore, this should be interpreted with caution. In the recent model, inclusion of an Aβ_{O} pool in the model could account for the differential effect of MBi-5 on Aβ40 and Aβ42 response observed in the data. In the Supplemental Material 3, the observed change in the ratio of Aβ42:Aβ40 after GS and BACE1 inhibition is presented. After GS inhibition, there is less difference in response of Aβ40 and Aβ42 observed, and thus less change in the ratio Aβ42:Aβ40. This may be caused by differential activation of some feedback mechanism on Aβ production or oligomerization, or model simplification of successive GS cleavage, as discussed above. Once quantitative data of Aβ_{O} response following BACE1 and GS is added, a difference in oligomerization may be confirmed.

Correction factors on Aβ42 and Aβ40 for study differences in study 1 and 2 compared to study 3, were implemented in the model on IPRED, assuming the underlying system is the same. Because these factors were implemented outside of the system, these are assumed to not affect model derived differences following GS *versus* BACE1 inhibition. The observed study variations in Aβ42 and Aβ40 levels could result from factors related to analytical procedures, such as differences in laboratory procedures among centers and technicians, sample handling or sample storage.

When planning a new study, a cross-over study design, in which each rhesus monkey receives MBi-5 and MK-0752, should be considered. This design will facilitate an adequate separation of study differences and differences in system responses following BACE1 or GS inhibition as the first is canceled out. Also, if sAPPα and sAPPβ response to GS inhibition would additionally be measured, it is anticipated that possible feedback

mechanism in the APP pathway can be further evaluated.

By challenging the model, we can learn something: If the existing model does not capture the data, we need to ask why and understand what is going. Subsequent model refinement can then be helpful in elucidating system behaviour and identifying knowledge gaps and further experiments.

Conclusions

The development of a systems pharmacology model is an evolutionary process, integrating knowledge of the biological system with emerging data. In the current analysis, by analysing the effects of two compounds with differing method of action, i.e. a GS and BACE1 inhibitor, acting on different sequence in the APP processing pathway, the APP processing pathway could be further elucidated. As a result, the systems pharmacology model of the APP pathway could be refined. The model characterized the response and inter-relationships of the APP metabolites and gave insight into the biological mechanisms of the system. The application of such a mechanistic approach that separates drug specific and systems specific parameters provides a robust characterization of the inhibitors. A differentiation in Aβ dynamics after BACE1 *versus* GS inhibition was found, reflected in a difference in Aβ40 formation. As such, the systems pharmacology analysis also points to parts of the APP system which require further investigation, in order to fully understand the interference of secretase inhibitors on the system.

References

1. van Maanen, E.M.T., *et al.* Systems pharmacology analysis of the amyloid cascade after β-secretase inhibition enables the identification of an Aβ42 oligomer pool. J Pharmacol Exp Ther. 2016;357(1):205–16.
2. Karran, E., Mercken, M., & De Strooper, B. The amyloid cascade hypothesis for Alzheimer's disease: an appraisal for the development of therapeutics. Nat Rev Drug Discov. 2011;10(9):698–712.
3. Husain, M.M., Kenneth, T., Siddique, H., & McClintock, S.M. Present and prospective clinical therapeutic regimens for Alzheimer's disease. Neuropsychiatr Dis Treat. 2008;4(4):765–777.
4. Cole, S.L. & Vassar, R. The basic biology of BACE1: A key therapeutic target for Alzheimer's disease. Curr Genomics. 2007;8(8):509–530.
5. Esler, W.P. & Wolfe, M.S. A portrait of Alzheimer secretases - New features and familiar faces. Science. 2001;293(5534): 1449–54.
6. Willem, M., *et al.* η-Secretase processing of APP inhibits neuronal activity in the hippocampus. Nature. 2015;526(7573):443–7.
7. Crump, C.J., *et al.* BMS-708,163 targets presenilin and lacks notch-sparing activity. Biochemistry. 2012;51(37):7209–11.
8. Martone, R.L., *et al.* Begacestat (GSI-953): a novel, selective thiophene sulfonamide inhibitor of amyloid precursor protein gamma-secretase for the treatment of Alzheimer's disease. J Pharmacol Exp Ther. 2009;331 (2):598–608.
9. Doody, R.S., *et al.* A phase 3 trial of semagacestat for treatment of Alzheimer's disease. N Engl J Med. 2013;369(4):341–50.
10. Das, R., *et al.* Modeling effect of a γ-secretase inhibitor on amyloid-β dynamics reveals significant role of an amyloid clearance mechanism. Bull Math Biol. 2011;73 (1):230–47.
11. Niva, C., Parkinson, J., Olsson, F., van Schaick, E., Lundkvist, J., & Visser, S.a.G. Has inhibition of Aβ production adequately been tested as therapeutic approach in mild AD? A model-based meta-analysis of γ-secretase inhibitor data. Eur J Clin Pharmacol. 2013;69(6):1247–60.
12. Tai, L.M., *et al.* The dynamics of Aβ distribution after γ-secretase inhibitor treatment, as determined by experimental and modelling approaches in a wild type rat. J Pharmacokinet Pharmacodyn. 2012;39(3):227–37.
13. Klein, W.L. Synaptotoxic amyloid-β oligomers: a molecular basis for the cause, diagnosis, and treatment of Alzheimer's disease? J Alzheimer's Dis. 2013;33:S49–S65.
14. Benilova, I., Karran, E., & De Strooper, B. The toxic Aβ oligomer and Alzheimer's disease: an emperor in need of clothes. Nat Neurosci. 2012;15(3):349–357.
15. Rosenblum, W.I. Why Alzheimer trials fail: removing soluble oligomeric beta amyloid

is essential, inconsistent, and difficult. Neurobiol Aging. 2014;35(5):969–974.

16. Cook, J.J., *et al.* Acute γ-secretase inhibition of nonhuman primate CNS shifts amyloid precursor protein (APP) metabolism from amyloid-β production to alternative APP fragments without amyloid-β rebound. J Neurosci. 2010;30(19):6743–50.

17. Gilberto, D.B., *et al.* An alternative method of chronic cerebrospinal fluid collection via the cisterna magna in conscious rhesus monkeys. Contemp Top Lab Anim Sci. 2003;42 (4):53–59.

18. Dobrowolska, J.A., *et al.* CNS amyloid-β, soluble APP-α and -β kinetics during BACE inhibition. J Neurosci. 2014;34(24): 8336–8346.

19. Wu, G., Sankaranarayanan, S., Hsieh, S.H.K., Simon, A.J., & Savage, M.J. Decrease in brain soluble amyloid precursor protein β (sAPPβ) in Alzheimer's disease cortex. J Neurosci Res. 2011;89(6):822–32.

20. Sankaranarayanan, S., *et al.* First demonstration of cerebrospinal fluid and plasma Aβ lowering with oral administration of a β-site amyloid precursor protein-cleaving enzyme 1 inhibitor in nonhuman primates. J Pharmacol Exp Ther. 2009;328(1):131–140.

21. Bauer, R.J. 2011 NONMEM users guide. Introduction to NONMEM 7.2.0 Technical report;ICON Development Solutions, Ellicott City, MD.

22. Iwatsubo, T., Odaka, A., Suzuki, N., Mizusawa, H., Nukina, N., & Ihara, Y. Visualization of Aβ42(43) and Aβ40 in senile plaques with end-specific Aβ monoclonals: evidence that an initially deposited species is Aβ42(43). Neuron. 1994;13(1):45–53.

23. Matsumura, N., *et al.* γ-Secretase associated with lipid rafts: multiple interactive pathways in the stepwise processing of β-carboxyl-terminal fragment. J Biol Chem. 2014;289(8):5109–21.

24. Tian, Y., Crump, C.J., & Li, Y.M. Dual Role of α-Secretase Cleavage in the Regulation of γ-Secretase Activity for Amyloid Production. J Biol Chem. 2010;285(42): 32549–32556.

25. Lichtenthaler, S.F. Alpha-secretase in Alzheimer's disease: Molecular identity, regulation and therapeutic potential. J Neurochem. 2011;116(1):10–21.

Chapter 5

Supplemental Material

Supplement to

Extending a systems model of the APP pathway: Separation of β- and γ-secretase sequential cleavage steps of APP

E.M.T. van Maanen, T.J. van Steeg, M.J. Ahsman, M.S. Michener, M.J. Savage, M.E. Kennedy, H.J. Kleijn, J.A. Stone, M. Danhof

Submitted to JPET

SUPPLEMENTAL MATERIAL (1)

Pharmacokinetic Data Analysis MK-0752

A population PK model was developed that describes the PK of MK-0752 in plasma and CSF in cisterna magna ported (CMP) rhesus monkeys. The results of the PK analysis of MK-0752 were used to predict target site exposure for each PD observation in the subsequent PK-PD analysis.

The PK model was developed and fitted to the data by means of non-linear mixed effects modeling using the NONMEM software package version VI level 2 (see the Materials and Methods section in Chapter 5).

The compartmental PK model of MK-0752 was based on the model reported by Shou *et al.* (2005)[1]. They reported that MK-0752 exhibits enterohepatic recirculation (EHR) in rhesus monkeys. Their four-compartment PK was modified for the simultaneous analysis of plasma and CSF PK data.

The PK profiles of MK-0752 in plasma and CSF were adequately described by a model containing six compartments: GI tract, central, peripheral, gall bladder, central CSF and peripheral CSF compartment (Supplemental Figure S5.1). The CSF compartment is linked to the central compartment, with input to CSF determined by the rate constant K_{in}. A peripheral CSF compartment is linked to the central CSF compartment, with exchange determined by the rate constants K_{63} and K_{36}. The model considered EHR of MK-0752 for which the recirculation rate from the gal bladder was described by a cosine function (Supplemental Equation S5.1):

$$CS = AMP \cdot COS\left(\frac{2\pi \cdot time}{PER} + HOR\right) + VER \tag{S5.1}$$

in which *AMP* is the amplitude of the cosine function corresponding to the maximum recirculation rate, *PER* is the period of the cosine function, *HOR* is the horizontal shift of the cosine function corresponding to a shift on the time axis and *VER* is the vertical shift of the cosine function corresponding to a shift on the rate axis.

The rate of change in each compartment can be expresses as:

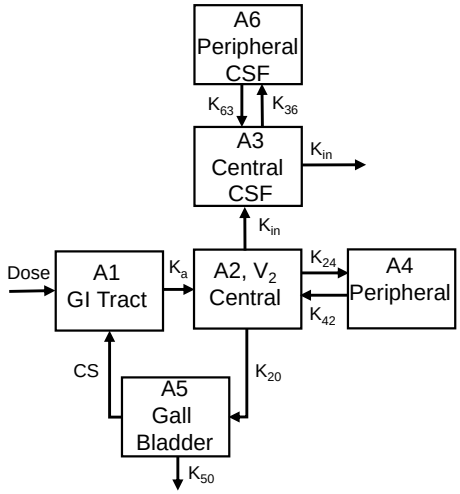

Figure S5.1: Schematic of the population PK model for MK-0752, that comprised of a GI tract, central, peripheral, gall bladder, central CSF and peripheral CSF compartment.
Rate constants for the individual compartments are K_a (absorption), K_{24} (rate constant from central to peripheral), K_{42} (rate constant from peripheral to central), K_{36} (rate constant from central CSF to peripheral CSF), K_{63} (rate constant from peripheral CSF to central CSF), K_{20} (rate constant from central to gall bladder), K_{50} (elimination rate from the gall bladder compartment), *CS* (rate constant recirculation via a cosine-function), K_{in} (rate constant from central to central CSF and elimination rate from the central CSF compartment). *A1*, *A2*, *A3*, *A4*, *A5* and *A6* are amounts (A) of MK-0752 in GI tract, central, central CSF, peripheral, gall bladder and peripheral CSF compartments, respectively. V_2 is the volume of the central compartment.

$$\frac{d}{dt}A_1 = -K_a \times A_1 + CS \times A_5 \tag{S5.2}$$

$$\frac{d}{dt}A_2 = K_a \times A_1 - K_{24} \times A_2 + K_{42} \times A_4 - K_{20} \times A_2 \tag{S5.3}$$

$$\frac{d}{dt}A_3 = K_{in} \times \frac{A_2}{V_2} - K_{36} \times A_3 + K_{63} \times A_6 - K_{in} \times A_3 \tag{S5.4}$$

$$\frac{d}{dt}A_4 = K_{24} \times A_2 - K_{42} \times A_4 \tag{S5.5}$$

$$\frac{d}{dt}A_5 = K_{20} \times A_2 - CS \times A_5 - K_{50} \times A_5 \tag{S5.6}$$

$$\frac{d}{dt}A_6 = K_{36} \times A_3 - K_{63} \times A_6 \tag{S5.7}$$

Table S5.1 shows all PK parameter estimates. The CSF input rate (K_{in}) could not be estimated with good precision. Considering the limitations of the data, this was accepted. The relative bioavailability (*F1*) was fixed to the value reported by Shou et al. (2005). The parameters *Ka* and *AMP* were fixed to parameter estimates from a preliminary analysis based on 60 mg/kg data only and a one compartmental model. In the two compartmental model based on 60 mg/kg and 240 mg/kg data, these could not be reliably estimated.

Interanimal variability was quantified for the clearance (*CL*) and volume of the central compartment (V_2). Residual variability (proportional error) was higher for the CSF than for the plasma concentration (0.173 and 0.132 for CSF and plasma, respectively).

The developed PK model gives an adequate description of plasma and CSF concentration time profiles, as can be seen from plots of the simulated and observed concentrations *versus* time profiles with 90% confidence interval (Supplemental Figure S5.2).

There is substantial CSF exposure after oral dosing, as shown by the PK data from the CMP rhesus monkeys. The data suggest that MK-0752 concentrations in brain, expected to be in between plasma and CSF levels, are sufficient to adequately inhibit γ-secretase activity in brain. The plasma and CSF concentrations *versus* time profiles predicted from the model were in good agreement with the values observed in the rhesus monkeys. Thus, the model could serve as input for PD model analysis.

Table S5.1: Population parameter estimates including coefficient of variation (CV%) for the PK model of MK-0752

PARAMETER	DESCRIPTION	VALUE	UNIT	CV%
Structural parameters				
K_a[a]	absorption rate	1.13	h^{-1}	-
CL	clearance	0.774	L/h	12.3
V_2	central volume	3.68	L	17.6
K_{24}	rate constant from central to CSF	0.00745	h^{-1}	27.8
K_{42}	rate constant from central to CSF	0.0229	h^{-1}	4.89
F1[a]	relative bioavailability	0.89	-	-
PER[a]	period of cosine function	24	h	-
AMP[a]	amplitude of cosine function	1.87	-	-
HOR	horizontal shift of cosine function	2.47	-	6.92
VER[a]	vertical shift of cosine function	0	-	-
K_{50}	elimination rate gall bladder compartment	1.02	h^{-1}	35.8
K_{in}CSF $\times$1000	CSF input and output rate	0.0381	h^{-1}	82.7
K_{36} as fraction of K_{in}	rate constant from central CSF to peripheral CSF as fraction of K_{in}	110	-	5.81
K_{63}	rate constant from peripheral CSF to central CSF	0.000926	h^{-1}	19.4
Interanimal variability				
ω_2^{CL}	Interanimal variability clearance	0.141		34.3
ω_2^{V2}	Interanimal variability central volume	0.381		37.3
$\omega_{(CL,V2)}$	Covariance between CL and V_2	0.195		33.3
Residual error				
σ^2_{plasma}	Residual variabiliy plasma	0.132		14.4
σ^2_{CSF}	Residual variabiliy CSF	0.173		12.2

[a] Fixed.

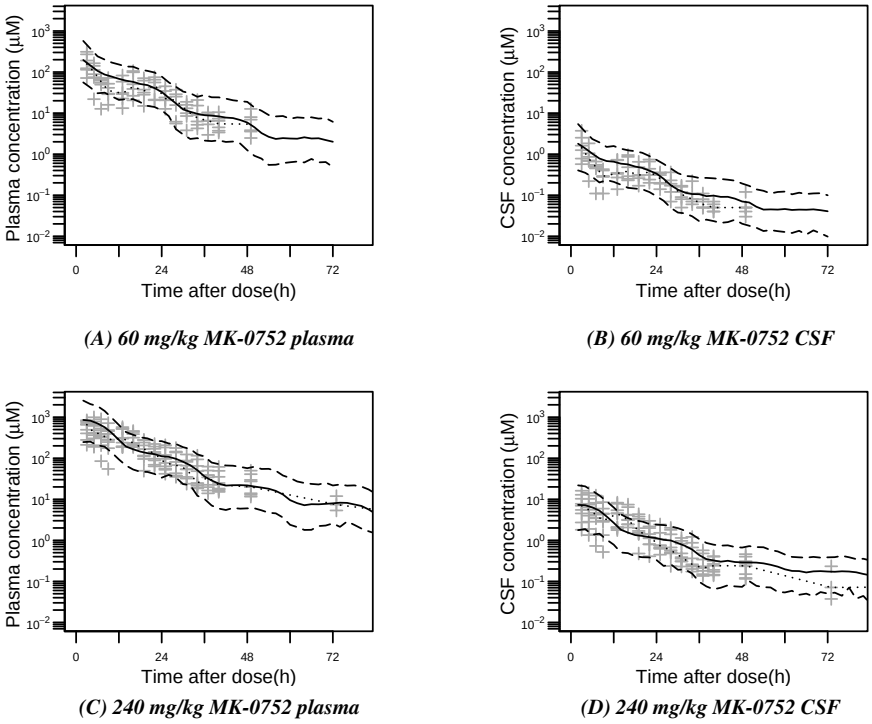

(A) 60 mg/kg MK-0752 plasma ***(B) 60 mg/kg MK-0752 CSF***

(C) 240 mg/kg MK-0752 plasma ***(D) 240 mg/kg MK-0752 CSF***

Figure S5.2: Visual predictive check of plasma* (left panels) *and CSF* (right panels) *concentration time profile of MK-0752 in the rhesus with 90% confidence interval. The rhesus were administrated with 60 mg/kg (A) (B) and 240 mg/kg (C) (D) MK-0752. Observation sample size: *Study 1*: n=16 for plasma and CSF per dose (60 and 240 mg/kg) from 6 monkeys collected over 2 days. *Study 2*: n=21 for plasma and CSF from 6 dose 240 mg/kg treated monkeys collected over 10 days. In the figure, the first 3 treatment days of study 2 are depicted. Plus-symbols represent observed measurements. Dotted line corresponds to the median observed profile. Solid lines show the median simulated profiles. The longs-dashed lines correspond to the 90% prediction intervals obtained from 1000 individual simulated profiles.

References

1. Shou, M., *et al.* Population pharmacokinetic modeling for enterohepatic recirculation in Rhesus monkey. Eur J Pharm Sci. 2005;26 (2):151–61.

SUPPLEMENTAL MATERIAL (2)

Study differences in Aβ baseline levels

Baseline data of Aβ40 and Aβ42 from the two GS inhibitor studies (study 1 and 2) and the BACE1 inhibitor study (study 3) is depicted in Fig. S5.3A and S5.3B, respectively, together with additional baseline data which was included in the analysis from study A and B. A large between-study variability in the baseline data was observed.

There was overlap in the rhesus monkey individuals included in the studies. Half of the subjects included in the GS inhibitor studies (study 1 and 2) was also used in the BACE1 inhibitor study (study 3) and study A.

In study time lines, Study B was run first, followed closely by study 1. Approximately 1 year later study 2 was conducted. Study A came next a few months later and lastly study 3 followed. No relationship between the age of the rhesus monkeys and the baseline level could be identified. As clock times were not available, a circadian rhythm in the combined baseline data could not be investigated.

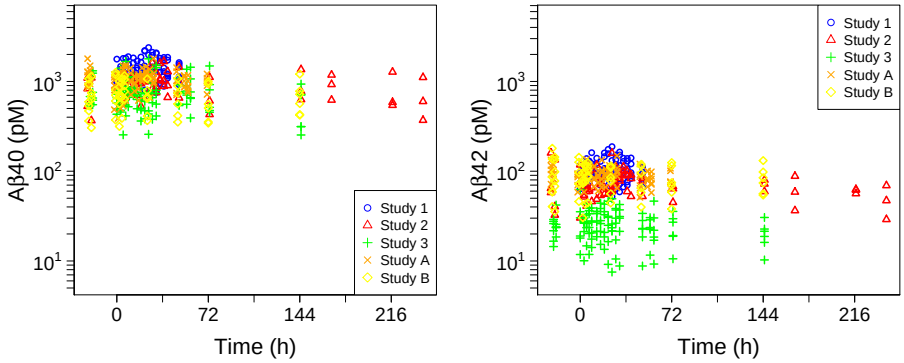

(A) Aβ40 *(B) Aβ42*

***Figure S5.3: Study differences in baseline levels of Aβ40* (left) *and Aβ42* (right).**

SUPPLEMENTAL MATERIAL (3)

Study differences in ratio Aβ42:Aβ40

The ratio Aβ42:Aβ40 from the two GS inhibitor studies (study 1 and 2) and the BACE1 inhibitor study (study 3) is depicted in Fig. S5.4A, S5.4B and S5.4C, respectively. BACE1 inhibition resulted in a bigger change in the ratio, compared to GS inhibition, with the investigated dosages.

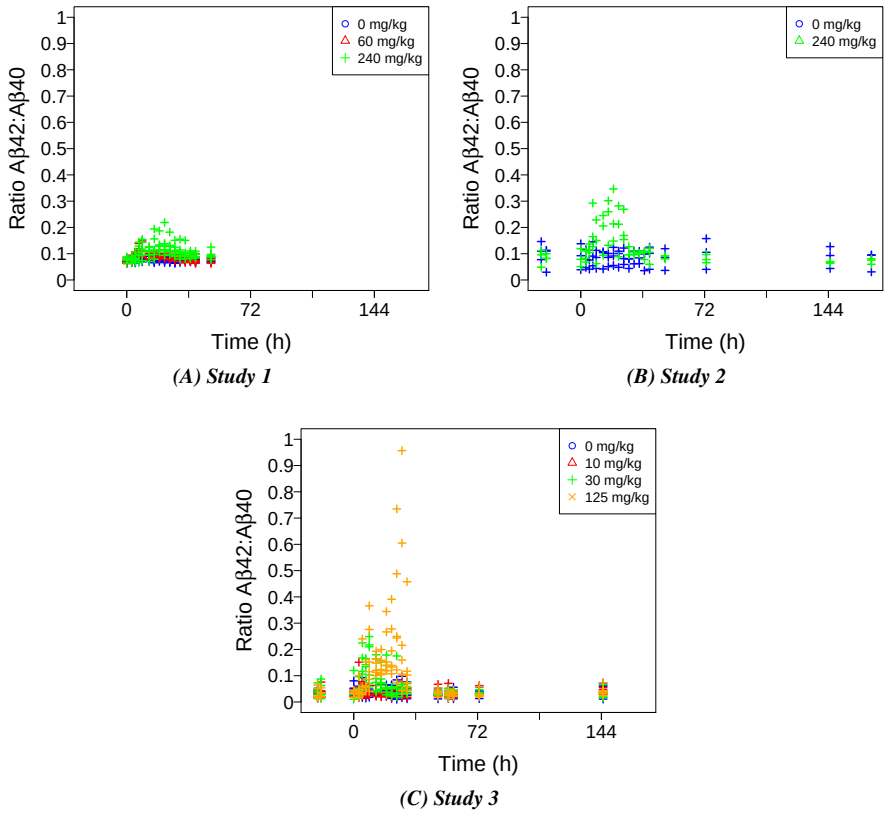

(A) Study 1 *(B) Study 2*

(C) Study 3

Figure S5.4: Study differences in the ratio Aβ42:Aβ40.